Letter

Bound on hot-spot mix in high-velocity, high-adiabat direct-drive cryogenic implosions based on comparison of absolute x-ray and neutron yields

R. C. Shah,[1,*] D. Cao,[1] L. Aghaian,[2] B. Bachmann,[3] R. Betti,[1] E. M. Campbell,[1] R. Epstein,[1] C. J. Forrest,[1] A. Forsman,[2] V. Yu. Glebov,[1] V. N. Goncharov,[1] V. Gopalaswamy,[1] D. R. Harding,[1] S. X. Hu,[1] I. V. Igumenshchev,[1] R. T. Janezic,[1] L. Keaty,[2] J. P. Knauer,[1] D. Kobs,[2] A. Lees,[1] O. M. Mannion,[1] Z. L. Mohamed,[1] D. Patel,[1] M. J. Rosenberg,[1] W. T. Shmayda,[1] C. Stoeckl,[1] W. Theobald,[1] C. A. Thomas,[1] P. Volegov,[4] K. M. Woo,[1] and S. P. Regan[1]

[1]*Laboratory for Laser Energetics, University of Rochester, Rochester, New York 14623, USA*

[2]*General Atomics, San Diego, California 92121, USA*

[3]*Lawrence Livermore National Laboratory, Livermore, California 94551, USA*

[4]*Los Alamos National Laboratory, Los Alamos, New Mexico 87545, USA*

(Received 2 October 2021; accepted 29 June 2022; published 15 July 2022)

In laser-driven implosions for laboratory fusion, the comparison of hot-spot x-ray yield to neutron production can serve to infer hot-spot mix. For high-performance direct-drive implosions, this ratio depends sensitively on the degree of equilibration between the ion and electron fluids. A scaling for x-ray yield as a function of neutron yield and characteristic ion and electron hot-spot temperatures is developed on the basis of simulations with varying degrees of equilibration. We apply this model to hot-spot x-ray measurements of direct-drive cryogenic implosions typical of the direct-drive designs with best ignition metrics. The comparison of the measured x-ray and neutron yields indicates that hot-spot mix, if present, is below a sensitivity estimated as ∼2% by-atom mix of ablator plastic into the hot spot.

DOI: 10.1103/PhysRevE.106.L013201

Direct-drive experiments of inertial confinement fusion (ICF) [1] are primarily studied on the 30-kJ, ∼30-TW OMEGA Laser System at the University of Rochester. Implosions at this scale are too small for appreciable alpha deposition, to allow for self-heating, but provide a hydrodynamic surrogate for scaling to larger systems such as the 1.9-MJ National Ignition Facility (NIF). Recently, a statistical approach has been developed to address gaps between models and the cryogenic direct-drive–implosion experiments [2]. The use of this statistically informed model has moved the program toward larger capsules that increase laser coupling (implosion velocity) at the expense of increased asymmetry due to the laser beam geometry [3,4]. The new designs have also increased the adiabat α, the ratio of pressure to the minimum Fermi pressure, which mitigates instability growth rates but reduces theoretical compression. The improved performance leads to conditions that are hydrodynamically equivalent to modest self-heating but insufficient for ignition.

Most recently, a physical basis has been ascribed to factors in the statistical model [5]. The neutron-yield production referenced to 1D calculation [yield over clean (YOC)] has been quantitatively ascribed to factors accounting for (1) implosion asymmetry primarily described by $\ell = 1$ Legendre modes of the drive in a spherical harmonic basis; (2) fuel aging that replaces tritium in the central vapor with helium-3; (3) beam-to-target size; and (4) hydrodynamic stability. In fact, 2D simulations indicate beam modes driven by beam-to-target size may couple to higher modes [6], suggesting a link to hydrodynamic instability for 50% to 60% of the performance gap from 1D (see examples in Table I). Hydrodynamic instabilities may lead to hot-spot "mix", or the presence of undesired ablator plastic in the central high-temperature DT plasma. Hot-spot mix will increase radiative cooling, and its presence or absence adds a constraint for physics models in multidimensional simulations. For direct-drive cryogenic implosions, mix has been characterized previously on slower implosions as a relative increase of x-ray emission as the adiabat was reduced [7] or more recently using specialized cryogenic targets with Ge-doped ablator [8].

Here we report on new continuum x-ray measurements to characterize hot-spot x-ray yield and hot-spot electron temperature of a series of implosions typical of current best cryogenic designs. The objective of these measurements is to consider the consistency of x-ray production relative to neutron production and assess if this ratio implies hot-spot mix. Because of the insufficient time for equilibration given plasma parameters in these high-velocity implosions, there are significant differences between the hot-spot electron and ion temperature, which can influence the comparison of the yields. Based on the measured neutron yield and both hot-spot temperatures, the expected x-ray yield (assuming a pure-DT hot spot) is determined for each implosion and then compared to the measured x-ray yield. The x-ray and neutron yields are found to be consistent without invoking hot-spot mix within an estimated sensitivity corresponding to ∼2% by-atom fully ionized carbon–deuterium plastic.

First, we will briefly summarize the concept of the use of continuum x-ray yield to assess hot-spot mix by comparison to neutron yield. This has been well documented in the literature

*rahulshah@lle.rochester.edu

TABLE I. Measured neutron yield relative to 1D (YOC) and contributions attributed by the statistical method [5] to fuel age (YOC_f), low mode asymmetry ($YOC_{\ell=1}$), beam-to-target ratio (YOC_b) and 1D hydrodynamic stability factors (YOC_h). Note that these partitions are based on ensemble statistics over the database and thus when multiplied are close to, but not necessarily equal to the measured YOC.

Shot	Y ($\times 10^{14}$)	YOC	YOC_f	$YOC_{\ell=1}$	YOC_b	YOC_h
96804	0.86	0.25	0.77	0.82	0.69	0.63
96806	1.56	0.41	0.89	1	0.66	0.62
96808	1.33	0.38	0.75	1	0.66	0.64
96811	1.43	0.37	0.88	1	0.66	0.65
96814	1.36	0.30	0.76	1	0.62	0.65

under the assumption of equilibrium conditions [7,9]. The key idea is that the x-ray and neutron production both depend on the hot-spot density and temperature conditions, but only the x rays are sensitively increased by high-Z contamination. The x-ray emissivity is a function of the local electron temperature (T_e), whereas the D–T fusion reactivity depends on ion collisions and therefore, the ion temperature (T_i). In the previous work, an assumption was that of equilibruim, i.e., T_e=T_i. With an assumed temperature profile and isobaric conditions, a hot-spot model can be constrained using the measured neutron yield and T_i. This hot-spot model, assuming pure DT ("no-mix") conditions, is used to compute the expected x-ray yield, which is then compared to the measured x-ray yield. If a mix of plastic into the hot spot occurs, then it will enhance the x-ray emissivity primarily due to $\langle Z^2 \rangle$ dependence of bremsstrahlung and $\langle Z^4 \rangle$ dependence of recombination emission (C, Z = 6).

For the direct-drive implosions of interest here, however, the equilibration is predicted to be incomplete (see Fig. 1(a), which shows temperature profiles at bang time as modeled by the 1D radiation-hydrodynamic code *LILAC* [10]). During the evolution of the hot spot, shocks preferentially heat the more-massive ions, with energy passing to the electrons via their collisions with the ions. The equilibration time τ_{eq} scales as $T_e^{3/2}/\rho$, where ρ is the density [1]. The high velocities of the new designs not only reduce the total time available for equilibration but also reduce equilibration via higher temperatures (this increases both τ_{eq} and losses due to the electron heat conduction $\chi \sim T_e^{5/2}$ [1,11]). Also suppressing equilibration in the modern implosions is the reduced compression accompanying higher adiabats. The impact of calculating the x-ray production with T_e as compared to an assumed T_i profile is plotted in Fig. 1(b) and shows that a single temperature model is inadequate. Here the x-ray energy of 15 keV was chosen because it results in a temperature dependence nearly matched to that of the DT fusion reactivity [11] [shown by the x-ray emission calculated using T_i in Fig. 1(b)].

From this discussion, an estimate of the expected x-ray production requires knowledge of both ion and electron temperature profiles (and an assumption of the density profile, usually taken as isobaric). At present, however, only integrated hot-spot values can be measured for each of these temperatures. If a simulation matched these temperatures,

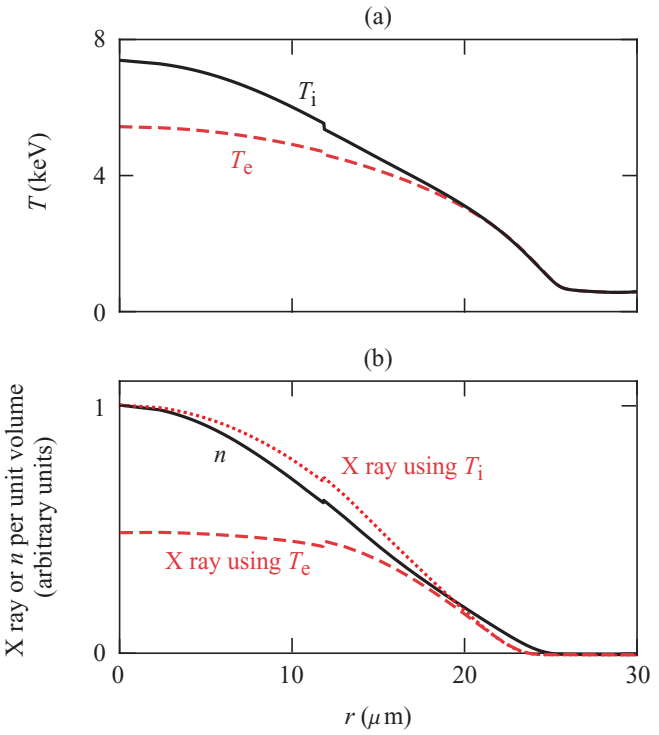

FIG. 1. (a) The electron and ion temperature profiles from 1D *LILAC* (shot 90288) at the time of peak neutron production show nonequilibrium conditions. (b) The peak value and profile of the x-ray (15-keV) production depends significantly on the degree of equilibration. The two different x-ray curves are identically normalized.

then we might assume the relationship between the x-ray and neutron source profiles to be as calculated. An extension of this idea is to use simulations of implosions with an assortment of thermal conditions to create a more-general scaling of x-ray to neutron yield. To do this we have used a database of 1D and 2D simulations of actual implosions on OMEGA [6] (calculated using the *DRACO* radiation-hydrodynamic code [12]). The uniform (1D) simulations, with equilibrations spanning from ~60% to 96%, have been used to relate x-ray yield (Y_x) to three experimentally measurable parameters: the DT neutron yield Y_n, T_i, and T_e (the density dependence is identical for the neutron and x-ray production). Assuming the temperature dependencies can be described as power laws, the best-fit mapping was determined from the 1D simulation ensemble as $Y_x = 2.4 \times 10^{-3} T_e^{3.9} T_i^{-2.25} Y_n$, where Y_x is in units of J/sr/keV and evaluated at 15 keV and temperatures are in units of keV. To be consistent with measurements, T_i is a neutron-weighted quantity, whereas Y_x and T_e are inferred from the calculated x-ray emission as detailed later. The simulated x-ray yield (extracted from post-processing) is divided by the "predicted" x-ray yield obtained from this scaling to determine an "x-ray enhancement" (see Fig. 2, solid black circles). This fit is then tested on companion 2D simulations (red asterisks), which include typical values of DT layer roughness [13], offset, laser beam power balance, and geometric effects due to finite beam profiles captured with a 3D ray trace. An analytic model describes laser imprint (to Legendre modes $\ell < 50$) and accounts for conditioning by distributed phase

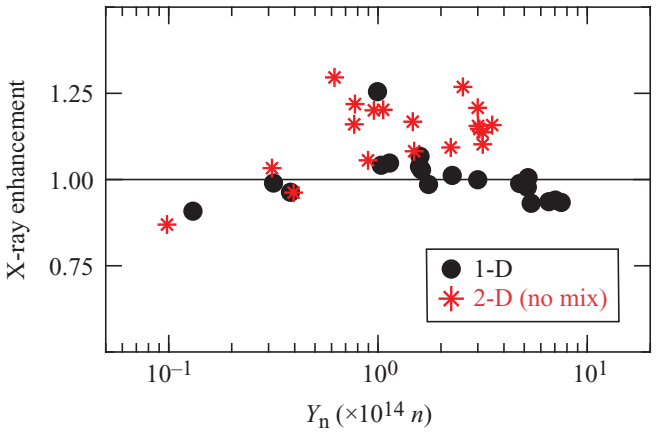

FIG. 2. Using 1D simulations with varying degrees of equilibration, a scaling was developed between neutron and x-ray yield that includes a dependence on hot-spot T_e and T_i (see text for details). The x-ray enhancement is defined as the x-ray yield directly obtained from the simulation divided by mapped x-ray yield. Since there is no hot-spot mix in either the 1D or 2D simulations, the residual deviations from unity here indicate systematic error and limits on the sensitivity of the mix inference.

plates [14,15], polarization rotation [16], and smoothing by spectral dispersion [17,18]. There is no hot-spot mix in these 2D simulations; thus, the x-ray enhancement ideally should be unity. The spread of the x-ray enhancement around unity in Fig. 2 shows limits of our assumptions and model. This spread in the modeled x-ray enhancement obtained with the range of simulations will be interpreted as indicative of model-imposed limitation in sensitivity of the analysis.

The data presented here come from the series of five cryogenic implosions that occurred on 25 February 2020 and are listed in Table I. The targets and laser drives were similar to what was used to reach the optimum with respect to ignition reported by Gopalaswamy *et al.* [2]. The total laser energy was 27.4 to 27.7 kJ. The targets had outer diameters of 954 to 979 μm with CD ablators nominally of 8-μm thickness (for the last shot the outer 3 μm included 6% Si by atom) and with cryogenic DT layers nominally of 39 μm thickness. The 1D design velocities and adiabats had small ranges of ∼444 to 468 km/s and 4 to 4.7, respectively.

The x-ray yield and electron temperature measurements were newly developed for this experiment. Building on the approach used at the NIF [19], ∼30 images of each implosion were generated using an array of differentially filtered circular apertures and recorded on an absolutely calibrated image plate (IP) [20]. The imaging apertures (∼130-μm diameter) make it possible to distinguish the hot-spot x rays (∼60-μm source) from a background of neutrons and coronal x rays (the spatial identification of hot spot as compared to coronal x rays was corroborated with simulation data). The apertures were positioned 109.5 mm from the implosion center and projected with 19.5× magnification. The x rays were filtered with Al foils ranging from ∼0.1 to 1.3 mm (measured thicknesses with an accuracy of ±1 μm were used in calculations) in order to have four data channels [21]. There is an additional 508-μm Be blast shield protecting the apertures, a 254-μm Be vacuum window, and 1-μm Kapton filtration common to all the channels. After accounting for IP response, the mean recorded energies of the channels ranged from 10 to 18 keV. In this range, the dense fuel was optically thin, and the signal level was within the dynamic range of a single scan read of the IP so as to be consistent with the calibration. The channel measurements were used to constrain an isobaric hot-spot model of Betti *et al.* [22]. This model is defined by center values of the temperature and density, T_{e0} and ρ_0, and is self-similar with a radial coordinate which is normalized to the edge of the hot spot, R_{max}. The hot spot (assumed static over an interval Δt) is used to calculate the volume integrated bremsstrahlung x-ray continuum using the free–free emissivity for hydrogen given by Eq. (12) of Ref. [7], which describes radiated x-ray energy per unit time–volume–steradian–frequency:

$$\epsilon_\nu^{FF} = \frac{32}{3\sqrt{\pi}}\beta a_0^3 n_i^2 \sqrt{\frac{\chi_H}{h\nu}} e^{-h\nu/kT_e},$$

where $\beta = 0.87$ is an average energy parameter related to quantum mechanical effects, a_0 is the Bohr radius, n_i is the ion density, χ_H is the K-shell ionization energy of hydrogen, and k is Boltzman's constant. Two parameters describing the hot spot are constrained by comparison with the channel signals: T_{e0} and $\kappa = \rho_0(R_{max}^3 \Delta t)^{0.5}$. [Figures 3(a)–3(c) show examples of the data, measured and modeled channel signals, and inferred spectrum for shot 96806.] Finally, a neutron-weighted T_e (using the D–T reactivity [1]) is calculated to parametrize

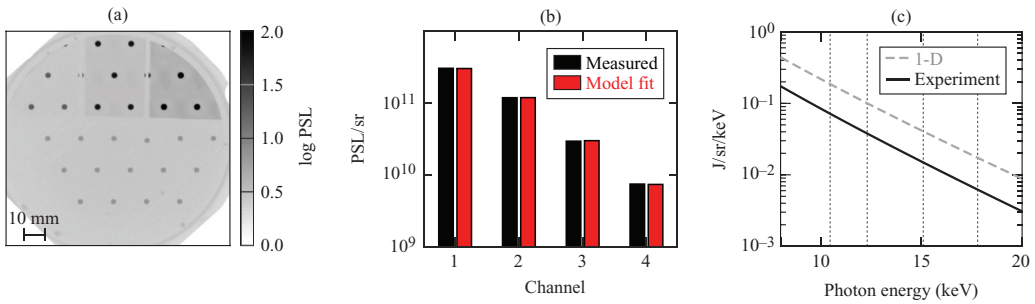

FIG. 3. (a) Image-plate data for shot 96806 with image intensity reported in units of photostimulated luminescence (PSL). (b) Measured and fit channel signals. (c) The hot-spot model x-ray spectrum determined from the channel data. Dotted vertical lines indicate the mean recorded energy of each of the four imaging channels. For reference, the hot-spot model x-ray spectrum obtained from the identical analysis of the 1D simulation is also plotted.

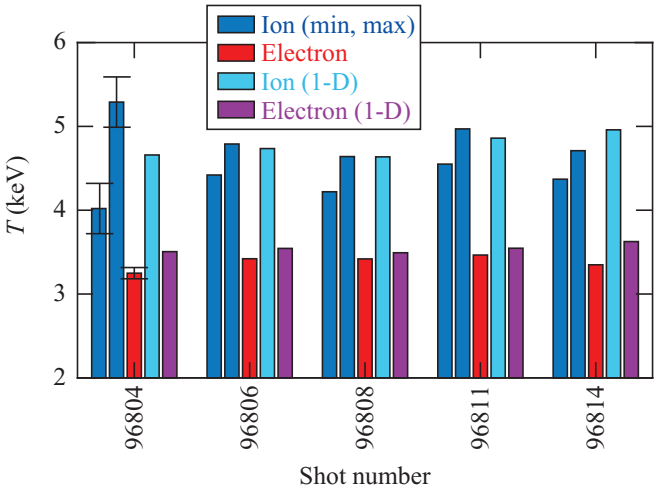

FIG. 4. The measured hot-spot T_e is typically ~75% of the minimum T_i obtained from five independent lines of sight. The result is similar to what is obtained from 1D simulations (and is thus a level of equilibration encompassed by the simulation database).

the hot-spot electron temperature on similar footing as the ion temperature. Sources of uncertainty are inferred from the multiple images and errors in foil thickness and IP response and are accounted for in forward propagation to the inferred quantities. For the simulations, post-processed x rays [23] were spatially and temporally selected to isolate the hot-spot contribution consistent with the measurement. The hot-spot x rays from the simulations were then filtered by the experimentally used channel responses and analyzed using the same procedure as for the data.

The measured hot-spot electron and ion temperatures, as well as the values from 1D simulation, are shown in the bar plot of Fig. 4. In contrast to the x-ray yield and electron temperature, neutron yield and ion temperature are routinely measured in ICF experiments on OMEGA. The hot-spot T_i is inferred based on the temporal width of the neutron time of flight (nTOF), which under ideal circumstances characterizes a neutron-weighted ion temperature by techniques outlined in Ref. [24]. This inferred T_i will be inflated by flows, which, if anisotropic, will result in variations of the inferred value as observed from different lines of sight [25]. In our experiments, there were five independent nTOF's and shown are the maximum and minimum values of T_i for each shot. The range between the extremes was large for only the first shot, for which a target defect was observed and believed to cause a large $\ell = 1$ flow. In that case, the minimum T_i takes its lowest value [and we observe the largest drop in neutron yield (see Table I)]. We have used the minimum nTOF T_i as the value best representative of the ion thermal conditions. Note from the Y_x prediction formula that an inflated value of T_i will reduce the expected x-ray yield; therefore in this sense the inferred mix quantification will be an upper bound estimate. Figure 4 also shows that the measured T_e value is typically ~75% of the minimum T_i. This degree of equilibration is similar to what is obtained in the 1D simulation (right two bars in Fig. 4).

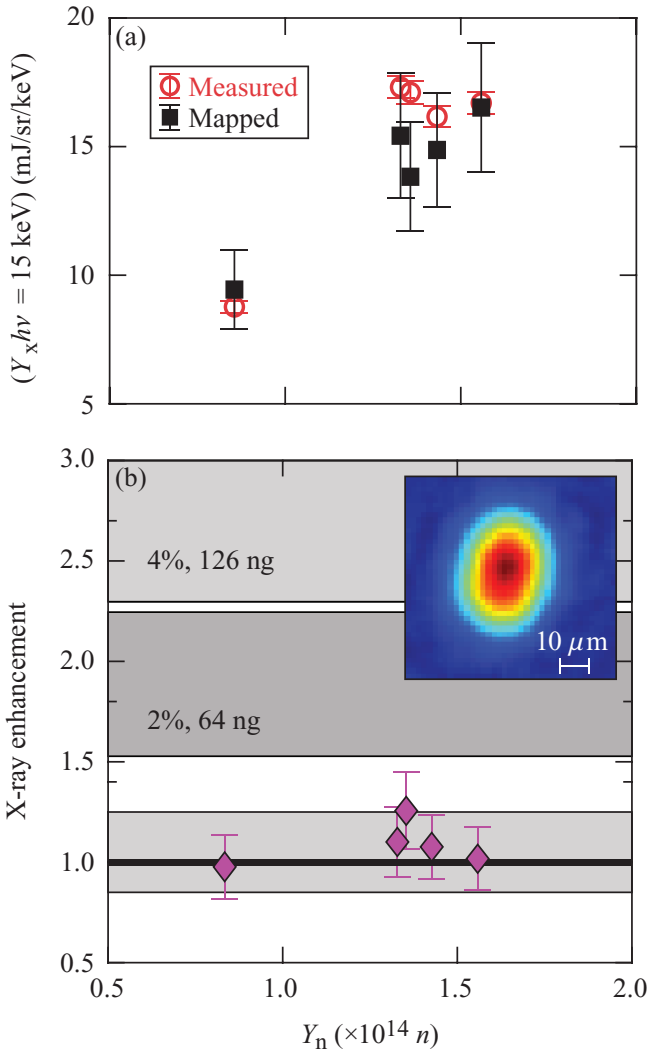

FIG. 5. (a) For each implosion, the measured Y_n, T_i, and T_e are used to calculate a mapped x-ray yield that is compared to the measured x-ray yield. (b) The x-ray enhancements fall within the systematic errors observed for the mapping (as determined by the simulation database) indicated by the shaded gray region of the plot (see also Fig. 2). The percentage values refer to percent-by-atom levels of CD mix required to cause the indicated level of x-ray enhancement. The mix mass in each case is determined assuming a typical hot-spot mass of 1.2 μg. (An x-ray enhancement, which is not included, will result from the 4% to 9% ^{3}He by atom in the vapor resulting from T decay. Our calculations indicate this may increase the emission by 6% to 14%.) The inset shows the recovered hot-spot image from Channel 1 for shot 96806.

The predicted Y_x for a hot spot in the absence of mix is calculated using these temperatures as well as the measured Y_n. This result, along with the measured Y_x, is plotted in Fig. 5(a). There is a generally positive correlation of the measured x-ray and neutron yields contrasting what was reported by Ma *et al.* [9] in indirect-drive implosions of the National Ignition Campaign and for which mix was identified as a prominent issue. Additionally, since the measured and mapped values of Y_x do not significantly deviate, there is no measurable indication that mix is consistently present across these implosions. This is

more explicitly shown in Fig. 5(b) as the ratio of the measured to mapped values, or x-ray enhancement. In this plot, the variability observed in the application of the model to the simulation database is indicated by the shaded region, and we interpret it as an estimate of the sensitivity by which we can measure an enhancement due to mix. Ranges are also indicated for specified fractions of mix in the hot spot, as determined using the formulas of Ref. [7], which account for the increase in both bremsstrahlung and recombination emission due to the carbon atoms. The measurement sensitivity is compromised by both the error propagation (dominated by the hot-spot temperatures and indicated with error bars) as well the model errors (indicated by the shaded region). We find no indication of hot-spot mix within the combined effect of these errors or an approximate sensitivity limited to $\sim$2% by atom carbon–deuterium (54 ng, assuming a typical 1.2-μg hot spot). We have also extracted the hot-spot images from the IP data using an established approximation to tomographic analysis [26,27], applicable for the precisely machined circular apertures (General Atomics, San Diego). The inset of Fig. 5(b) shows the image with an estimated 8 μm resolution obtained from Channel 1 for Shot 96806. Typical of all the implosions and other channels, we do not identify the sorts of bright features which have been associated with mix in other experiments [28–30]. It is plausible that decompression, peripheral bubbles, and residual motions previously proposed based on experimental signatures [31] dominate the hydrodynamic degradations without creating hot-spot mix. However, we cannot exclude the possibility of fine-scale jetted ablator material in the hot spot at levels below our sensitivity but which may still impact implosions, both through radiative losses and excess hot-spot mass [32].

In summary, measurements were presented of the x-ray yield and hot-spot electron temperature for direct-drive cryogenic implosion experiments. The comparison of the electron temperature with the ion temperature routinely characterized in the experiments was consistent with the prediction that ions and electrons remain substantially unequilibrated in the high-velocity, high-adiabat designs of present interest. The independently measured electron and ion temperatures of the hot spot with the D–T fusion neutron yield were used to estimate a corresponding x-ray yield expected from the nonequilibrium DT hot spot, assuming the absence of mix. The comparison of the measured and expected x-ray yields is consistent within the estimated sensitivity of the technique and therefore indicates that hot-spot mix, if present in these implosions, is at levels less than what the yield comparison can detect.

We acknowledge OMEGA Operations, OMEGA System Science, and LLE Engineering for implementation. Targets were prepared by LLE Target Fabrication and General Atomics (San Diego). D. Walker conducted IP calibrations. This work is supported by the Department of Energy National Nuclear Security Administration under Award No. DE-NA0003856, the University of Rochester, and the New York State Energy Research and Development Authority. This report was prepared as an account of work sponsored by an agency of the U.S. Government. Neither the U.S. Government nor any agency thereof, nor any of their employees, makes any warranty, express or implied, or assumes any legal liability or responsibility for the accuracy, completeness, or usefulness of any information, apparatus, product, or process disclosed, or represents that its use would not infringe privately owned rights. Reference herein to any specific commercial product, process, or service by trade name, trademark, manufacturer, or otherwise does not necessarily constitute or imply its endorsement, recommendation, or favoring by the U.S. Government or any agency thereof. The views and opinions of authors expressed herein do not necessarily state or reflect those of the U.S. Government or any agency thereof.

[1] S. Atzeni and J. Meyer-ter-vehn, *The Physics of Inertial Confinement Fusion* (Oxford University Press, Oxford, UK, 2004)

[2] V. Gopalaswamy, R. Betti, J. P. Knauer, N. Luciani, D. Patel, K. M. Woo, A. Bose, I. V. Igumenshchev, E. M. Campbell, K. S. Anderson, K. A. Bauer, M. J. Bonino, D. Cao, A. R. Christopherson, G. W. Collins, T. J. B. Collins, J. R. Davies, J. A. Delettrez, D. H. Edgell, R. Epstein *et al.*, Tripled yield in direct-drive laser fusion through statistical modelling, Nature (London) **565**, 581 (2019).

[3] D. H. Froula, I. V. Igumenshchev, D. T. Michel, D. H. Edgell, R. Follett, V. Y. Glebov, V. N. Goncharov, J. Kwiatkowski, F. J. Marshall, P. B. Radha, W. Seka, C. Sorce, S. Stagnitto, C. Stoeckl, and T. C. Sangster, Increasing Hydrodynamic Efficiency by Reducing Cross-Beam Energy Transfer in Direct-Drive-Implosion Experiments, Phys. Rev. Lett. **108**, 125003 (2012).

[4] I. V. Igumenshchev, V. N. Goncharov, F. J. Marshall, J. P. Knauer, E. M. Campbell, C. J. Forrest, D. H. Froula, V. Y. Glebov, R. L. McCrory, S. P. Regan, T. C. Sangster, S. Skupsky, and C. Stoeckl, Three-dimensional modeling of direct-drive cryogenic implosions on omega, Phys. Plasmas **23**, 052702 (2016).

[5] A. Lees, R. Betti, J. P. Knauer, V. Gopalaswamy, D. Patel, K. M. Woo, K. S. Anderson, E. M. Campbell, D. Cao, J. Carroll-Nellenback, R. Epstein, C. Forrest, V. N. Goncharov, D. R. Harding, S. X. Hu, I. V. Igumenshchev, R. T. Janezic, O. M. Mannion, P. B. Radha, S. P. Regan *et al.*, Experimentally Inferred Fusion Yield Dependencies of OMEGA Inertial Confinement Fusion Implosions, Phys. Rev. Lett. **127**, 105001 (2021).

[6] D. Cao *et al.*, Understanding origins of observed fusion yield dependencies (unpublished).

[7] R. Epstein, V. N. Goncharov, F. J. Marshall, R. Betti, R. Nora, A. R. Christopherson, I. E. Golovkin, and J. J. MacFarlane, X-ray continuum as a measure of pressure and fuel-shell mix in compressed isobaric hydrogen implosion cores, Phys. Plasmas **22**, 022707 (2015).

[8] S. P. Regan *et al.*, First observation of hot-spot mix in laser direct-drive inertial confinement fusion and its dependence on implosion adiabat (unpublished).

[9] T. Ma, P. K. Patel, N. Izumi, P. T. Springer, M. H. Key, L. J. Atherton, L. R. Benedetti, D. K. Bradley, D. A. Callahan, P. M. Celliers, C. J. Cerjan, D. S. Clark, E. L. Dewald, S. N. Dixit, T. Döppner, D. H. Edgell, R. Epstein, S. Glenn, G. Grim, S. W. Haan *et al.*, Onset of Hydrodynamic Mix in High-Velocity, Highly Compressed Inertial Confinement Fusion Implosions, Phys. Rev. Lett. **111**, 085004 (2013).

[10] J. Delettrez, R. Epstein, M. C. Richardson, P. A. Jaanimagi, and B. L. Henke, Effect of laser illumination nonuniformity on the analysis of time-resolved x-ray measurements in uv spherical transport experiments, Phys. Rev. A **36**, 3926 (1987).

[11] D. Cao, R. C. Shah, S. P. Regan, R. Epstein, I. V. Igumenshchev, V. Gopalaswamy, A. R. Christopherson, W. Theobald, P. B. Radha, and V. N. Goncharov, Interpreting the electron temperature inferred from x-ray continuum emission for direct-drive inertial confinement fusion implosions on omega, Phys. Plasmas **26**, 082709 (2019).

[12] S. X. Hu, V. N. Goncharov, P. B. Radha, J. A. Marozas, S. Skupsky, T. R. Boehly, T. C. Sangster, D. D. Meyerhofer, and R. L. McCrory, Two-dimensional simulations of the neutron yield in cryogenic deuterium-tritium implosions on omega, Phys. Plasmas **17**, 102706 (2010).

[13] D. H. Edgell, R. S. Craxton, L. M. Elasky, D. R. Harding, L. S. Iwan, R. L. Keck, L. D. Lund, S. J. Verbridge, M. D. Wittman, A. Warrick, T. Brown, and W. Seka, Three-dimensional characterization of cryogenic target ice layers using multiple shadowgraph views, Fusion Sci. Technol. **49**, 616 (2006).

[14] Y. Kato, K. Mima, N. Miyanaga, S. Arinaga, Y. Kitagawa, M. Nakatsuka, and C. Yamanaka, Random Phasing of High-Power Lasers for Uniform Target Acceleration and Plasma-Instability Suppression, Phys. Rev. Lett. **53**, 1057 (1984).

[15] T. J. Kessler, Y. Lin, J. J. Armstrong, and B. Velazquez, Phase conversion of lasers with low-loss distributed phase plates, in *Laser Coherence Control: Technology and Applications*, Vol. 1870, edited by H. T. Powell and T. J. Kessler, International Society for Optics and Photonics (SPIE, Los Angeles, CA, 1993), pp. 95–104.

[16] T. R. Boehly, V. A. Smalyuk, D. D. Meyerhofer, J. P. Knauer, D. K. Bradley, R. S. Craxton, M. J. Guardalben, S. Skupsky, and T. J. Kessler, Reduction of laser imprinting using polarization smoothing on a solid-state fusion laser, J. Appl. Phys. **85**, 3444 (1999).

[17] S. Skupsky and R. S. Craxton, Irradiation uniformity for high-compression laser-fusion experiments, Phys. Plasmas **6**, 2157 (1999).

[18] S. P. Regan, J. A. Marozas, J. H. Kelly, T. R. Boehly, W. R. Donaldson, P. A. Jaanimagi, R. L. Keck, T. J. Kessler, D. D. Meyerhofer, W. Seka, S. Skupsky, and V. A. Smalyuk, Experimental investigation of smoothing by spectral dispersion, J. Opt. Soc. Am. B **17**, 1483 (2000).

[19] L. C. Jarrott, B. Bachmann, T. Ma, L. R. Benedetti, F. E. Field, E. P. Hartouni, R. Hatarik, N. Izumi, S. F. Khan, O. L. Landen, S. R. Nagel, R. Nora, A. Pak, J. L. Peterson, M. B. Schneider, P. T. Springer, and P. K. Patel, Thermal Temperature Measurements of Inertial Fusion Implosions, Phys. Rev. Lett. **121**, 085001 (2018).

[20] M. J. Rosenberg, D. B. Thorn, N. Izumi, D. Williams, M. Rowland, G. Torres, M. Haugh, P. Hillyard, N. Adelman, T. Schuler, M. A. Barrios, J. P. Holder, M. B. Schneider, K. B. Fournier, D. K. Bradley, and S. P. Regan, Image-plate sensitivity to x rays at 2 to 60 kev, Rev. Sci. Instrum. **90**, 013506 (2019).

[21] NIST Standard Reference Database 126, https://dx.doi.org/10.18434/T4D01F.

[22] R. Betti, K. Anderson, V. N. Goncharov, R. L. McCrory, D. D. Meyerhofer, S. Skupsky, and R. P. J. Town, Deceleration phase of inertial confinement fusion implosions, Phys. Plasmas **9**, 2277 (2002).

[23] J. MacFarlane, I. Golovkin, P. Wang, P. Woodruff, and N. Pereyra, Spect3d - a multi-dimensional collisional-radiative code for generating diagnostic signatures based on hydrodynamics and pic simulation output, High Energy Density Phys. **3**, 181 (2007).

[24] T. J. Murphy, R. E. Chrien, and K. A. Klare, Interpretation of neutron time-of-flight signals from current-mode detectors, Rev. Sci. Instrum. **68**, 610 (1997).

[25] T. J. Murphy, R. E. Chrien, and K. A. Klare, Interpretation of neutron time-of-flight signals from expanding or contracting spherical sources, Rev. Sci. Instrum. **68**, 614 (1997).

[26] B. Bachmann, T. Hilsabeck, J. Field, N. Masters, C. Reed, T. Pardini, J. R. Rygg, N. Alexander, L. R. Benedetti, T. Döppner, A. Forsman, N. Izumi, S. LePape, T. Ma, A. G. MacPhee, S. Nagel, P. Patel, B. Spears, and O. L. Landen, Resolving hot-spot microstructure using x-ray penumbral imaging (invited), Rev. Sci. Instrum. **87**, 11E201 (2016).

[27] G. Di Domenico, P. Cardarelli, A. Contillo, A. Taibi, and M. Gambaccini, X-ray focal spot reconstruction by circular penumbra analysis-application to digital radiography systems, Med. Phys. **43**, 294 (2016).

[28] G. A. Kyrala, S. Dixit, S. Glenzer, D. Kalantar, D. Bradley, N. Izumi, N. Meezan, O. L. Landen, D. Callahan, S. V. Weber, J. P. Holder, S. Glenn, M. J. Edwards, P. Bell, J. Kimbrough, J. Koch, R. Prasad, L. Suter, J. L. Kline, and J. Kilkenny, Measuring symmetry of implosions in cryogenic *Hohlraums* at the NIF using gated x-ray detectors (invited), Rev. Sci. Instrum. **81**, 10E316 (2010).

[29] A. Pak, L. Divol, C. R. Weber, L. F. Berzak Hopkins, D. S. Clark, E. L. Dewald, D. N. Fittinghoff, V. Geppert-Kleinrath, M. Hohenberger, S. Le Pape, T. Ma, A. G. MacPhee, D. A. Mariscal, E. Marley, A. S. Moore, L. A. Pickworth, P. L. Volegov, C. Wilde, O. A. Hurricane, and P. K. Patel, Impact of Localized Radiative Loss on Inertial Confinement Fusion Implosions, Phys. Rev. Lett. **124**, 145001 (2020).

[30] B. Bachmann, J. E. Ralph, A. B. Zylstra, S. A. MacLaren, T. Döppner, D. O. Gericke, G. W. Collins, O. A. Hurricane, T. Ma, J. R. Rygg, H. A. Scott, S. A. Yi, and P. K. Patel, Localized mix-induced radiative cooling in a capsule implosion at the national ignition facility, Phys. Rev. E **101**, 033205 (2020).

[31] A. Bose, K. M. Woo, R. Betti, E. M. Campbell, D. Mangino, A. R. Christopherson, R. L. McCrory, R. Nora, S. P. Regan, V. N. Goncharov, T. C. Sangster, C. J. Forrest, J. Frenje, M. Gatu Johnson, V. Y. Glebov, J. P. Knauer, F. J. Marshall, C. Stoeckl, and W. Theobald, Core conditions for alpha heating attained in direct-drive inertial confinement fusion, Phys. Rev. E **94**, 011201(R) (2016).

[32] I. V. Igumenshchev, V. N. Goncharov, W. T. Shmayda, D. R. Harding, T. C. Sangster, and D. D. Meyerhofer, Effects of local defect growth in direct-drive cryogenic implosions on omega, Phys. Plasmas **20**, 082703 (2013).